

RSC Advances



This article can be cited before page numbers have been issued, to do this please use: D. Yu, J. bai, H. liang, J. wang and C. li, *RSC Adv.*, 2015, DOI: 10.1039/C5RA19235H.



This is an *Accepted Manuscript*, which has been through the Royal Society of Chemistry peer review process and has been accepted for publication.

Accepted Manuscripts are published online shortly after acceptance, before technical editing, formatting and proof reading. Using this free service, authors can make their results available to the community, in citable form, before we publish the edited article. This *Accepted Manuscript* will be replaced by the edited, formatted and paginated article as soon as this is available.

You can find more information about *Accepted Manuscripts* in the [Information for Authors](#).

Please note that technical editing may introduce minor changes to the text and/or graphics, which may alter content. The journal's standard [Terms & Conditions](#) and the [Ethical guidelines](#) still apply. In no event shall the Royal Society of Chemistry be held responsible for any errors or omissions in this *Accepted Manuscript* or any consequences arising from the use of any information it contains.



RSC Adv.

ARTICLE

A new fabrication of AgX (X= Br, I)-TiO₂ nanoparticles immobilized on polyacrylonitrile (PAN) nanofibers with high photocatalytic activity and renewable property

Dandan Yu,^a Jie Bai,^{*a} Haiou Liang,^a Junzhong Wang,^a and Chunping Li^aReceived 00th January 20xx,
Accepted 00th January 20xx

DOI: 10.1039/x0xx00000x

www.rsc.org/

A highly efficient visible light-driven AgX-TiO₂/PAN (X= Br, I) photocatalyst was synthesized by means of a combination of the electrospinning technique, solvothermal synthesis, physical adsorption and gas/solid reaction. The component, morphological and optical properties of the photocatalysts were characterized by X-ray diffraction (XRD), field-emission scanning electron microscopy (FE-SEM), transmission electron microscopy (TEM), UV-vis diffuse reflectance spectroscopy (DRS) and Fourier transform infrared spectroscopy (FTIR). The as-prepared composites exhibited the excellent photocatalytic efficiency for the degradation of methyl orange (MO), methylene blue (MB), acid red 18, sodium fluorescence, xylenol orange and phenol under visible light irradiation. Compared with pure PAN, AgX/PAN and TiO₂/PAN, AgX-TiO₂/PAN showed the much higher photocatalytic activity in degrading MO. In addition, AgX-TiO₂/PAN had a certain photochemical stability and could be regenerated easily. The application of PAN nanofibers made it easy separate the catalysts from an aqueous solution without any loss. The degradation of MO in the presence of different scavengers suggested that holes and •O₂⁻ were the main reactive species and holes played the predominant role. Thus, a possible two-stage photocatalytic mechanism associated with AgX-TiO₂/PAN was proposed.

Introduction

Currently, semiconductor photocatalysis has attracted remarkable attention in solving environment and energy problems.¹⁻⁴ From the semiconductor photocatalysts investigated, TiO₂ is considered to be a desirable material for the elimination of organic pollutants due to its high activity, stability, low cost and nontoxicity.⁵⁻⁷ However, the practical application of TiO₂ has been greatly hampered by the inefficient utilization of solar energy because of its wide band gap (anatase, 3.2 eV; rutile, 3.0 eV) and the rapid recombination of photogenerated electron-hole pairs.⁵⁻¹⁰ There are some different approaches to be explored to extend the absorption edge of TiO₂ into the visible region, such as nonmetal and metal doping,^{7,8} anionic or cationic doping,¹⁰ noble metal deposition¹¹ and coupling with other narrow band gap semiconductors.¹²

Silver halides (AgX, X= Br, I), the important narrow band gap semiconductors, have been recognized as photosensitive materials and extensively used in photographic films.¹³⁻¹⁵ Under light irradiation, silver halides absorb photons and electron-hole pairs can be liberated.^{15,16} The photogenerated electrons are easily captured by the Ag⁺, leading to formation of silver atoms (Ag⁰).¹⁴⁻¹⁶

In general, silver halides are unstable under light irradiation, which greatly affects their applications in photocatalytic reactions. Many researchers have reported that AgX could maintain its stability by coupling with other support materials such as TiO₂,¹⁶⁻²² ZnO²³⁻²⁵ and BiOX.^{5,26,27} Hu et al. have prepared AgI/TiO₂ photocatalysts by deposition-precipitation method and the catalyst's activity was maintained effectively for degradation of K-2G after six cycling runs under visible light irradiation without the destruction from AgI.¹⁶ According to previous researches, the photosensitivity of AgX makes it feasible to synthesize a novel photocatalyst by coupling AgX nanoparticles with TiO₂.

In addition, TiO₂ particles are easy to agglomerate and difficult to recover after being used for photocatalytic reactions.^{28,29} To overcome these hurdles, many efforts have been made to immobilize TiO₂ nanoparticles on various supporters such as zeolite,³¹ carbon nanofiber,³² carbon nanotubes³³ and graphene.^{30,34} Owing to the advantages of fine stability and easily availability,³⁶⁻³⁹ polyacrylonitrile (PAN) nanofibers obtained from an effective and economical electrospinning technique may be promising materials for the immobilization of catalysts as follows: (1) the large specific surface area is beneficial to the high exposure level of photocatalysts nanoparticles and further enhance the photocatalytic activity,^{28,35,39} (2) the randomly arrayed nanofibers favour the separation, recovery and reuse of photocatalysts,³⁹ (3) PAN nanofibers are hydrophobic with a low density and easily fixed at the proper position of the reactors, which could maximize the efficiency of light utilization by avoiding the hindrance of light penetration.²⁹ Su et al. have successfully fabricated TiO₂/PAN hybrid

^aChemical Engineering College, Inner Mongolia University of Technology, Huhhot 010051, People's Republic of China. E-mail: baijie@imut.edu.cn (J. Bai); Fax: +86 471 6575722; Tel.: +86 471 6575722.

† Footnotes relating to the title and/or authors should appear here. Electronic Supplementary Information (ESI) available: [details of any supplementary information available should be included here]. See DOI: 10.1039/x0xx00000x

ARTICLE

RSC Adv.

nanofibers by electrospinning and hydrothermal processes.³⁵ The as-prepared catalysts showed the high removal efficiencies of SO₂ and NO in the UV light photocatalysis oxidation of flue gas. Therefore, it is a great ideal to prepare a recyclable photocatalyst by immobilizing TiO₂ on the surface of PAN nanofibers.

Based on the above statements, a novel photocatalyst AgX (X = Br, I)-TiO₂ nanoparticles immobilized on PAN nanofibers were successfully prepared through the electrospinning, solvothermal synthesis,²⁹ physical adsorption process and gas/solid reaction.³⁸ In the present work, a series of photocatalysts with different molar ratio between AgX and TiO₂ had been fabricated and the photocatalytic activities of the as-prepared catalysts were evaluated by decomposing different organics (methyl orange, acid red 18, methylene blue, xylene orange, sodium fluorescein and phenol) under visible light irradiation. Moreover, a recycling test was conducted to investigate the photochemical stability and reusability of catalysts and a possible photocatalytic mechanism of the highly enhanced performance was also proposed.

Experimental Section

Materials

Polyacrylonitrile (PAN, M_w = 80 000) was purchased from Kunshan Hongyu Plastics Co., Ltd. N,N-dimethylformamide (C₃H₇NO, AR, 99.5%) was purchased from Tianjin Fuyu Fine Chemical Co., Ltd. Tetra-n-butyl titanate (Ti(OC₄H₉)₄, AR, 98.5%) was purchased from Xiya Reagent. Acetic acid (CH₃COOH, AR, 99.5%) was provided by Beijing Chemicals Co. Silver nitrate (AgNO₃, AR, 99.8%), absolute ethyl alcohol (C₂H₆O, AR, 99.7%) and bromine (Br₂, AR, 99.5%) were purchased from Sinopharm Chemical Reagent Co., Ltd. Iodine (I₂, AR, 99.8%) was supplied by Tianjin Chemical Reagent Factory. The above chemical reagents were used as received without further treatment.

Synthesis of TiO₂/PAN hybrid nanofibers

Polyacrylonitrile (PAN) was dissolved in N,N-dimethylformamide (DMF) with vigorous stirring to form a homogeneous 8 wt% PAN/DMF solution for the subsequent electrospinning process. The solution was placed in a glass dropper. A self-made copper ring was wrapped around the top of glass dropper and connected to the anode of a high voltage generator. The applied direct current voltage was 17 kV. A piece of aluminium foil connected to the cathode was placed in 15 cm distance from the tip of the dropper to collect PAN nanofibers. Secondly, 1 ml Tetra-n-butyl titanate (Ti(OC₄H₉)₄) and 0.15 ml acetic acid (CH₃COOH) were respectively added into 20 ml continuous stirred absolute ethyl alcohol. Then 0.15 g of PAN nanofibers was dispersed into the above mixture solution followed by 24 h physical adsorption. Subsequently, the mixtures were transferred into a 100 ml Teflon-lined stainless autoclave and kept at 180 °C for 9 h. After cooling to room temperature naturally, the products were collected, washed several times with water and dried at 80 °C for 2 h in a vacuum oven. Thus, TiO₂/PAN hybrid nanofibers were fabricated.

Preparation of AgX-TiO₂/PAN (X= Br, I) nanocomposites

AgX-TiO₂/PAN (X= Br, I) was synthesized as follows: 0.0250 g AgNO₃ was dissolved in 100 ml deionized water under dark condition. Then 0.4 g of TiO₂/PAN hybrid nanofibers was added subsequently by physical adsorption for 6 h with stirring constantly. The composites containing Ag⁺ were filtered, washed three times using deionized water and transferred to a vacuum oven to dry at 90 °C for 3 h. To prepare AgX-TiO₂/PAN, the obtained Ag (I)-TiO₂/PAN composites were exposed in I₂ atmosphere for 48 h (or Br₂ atmosphere for 24 h). Finally, they were placed in a vacuum oven to evaporate residual I₂ (or Br₂) at 90 °C for 4 h. And the as-prepared sample was named AgX (10%)-TiO₂/PAN. By changing the dosage of AgNO₃ to 0.0050 g, 0.0100 g, 0.0150 g and 0.0200 g, respectively, a series of AgX-TiO₂/PAN photocatalysts was prepared and labeled as AgX (y%)-TiO₂/PAN, where y% represents the molar ratio of AgX/TiO₂. For comparison, AgX/PAN (X= Br, I) was synthesized through similar processes by using 0.0250 g AgNO₃ and 0.3 g PAN without solvothermal treatment.

Characterization

To study the crystal phase and crystalline of the samples, X-ray diffraction (XRD, Rigaku Ultima IV, Japan) patterns were performed in a range of 2θ from 10° to 90° with a scanning rate of 2°/min. The morphologies of the products were observed by field-emission scanning electron microscopy (FE-SEM, FEGQUANTAN 650) and transmission electron microscopy (TEM, F20 S-TWIN, Tecnai). The UV-vis diffuse reflectance spectra (DRS) were measured with a Shimadzu UV (3600)-vis spectrophotometer and BaSO₄ was used as a reference material. Fourier transform infrared spectra (FTIR) were recorded from KBr pellet in a Nicolet Nexus 670 spectrophotometer with a range of 400-4000 cm⁻¹.

Photocatalytic performance

The photocatalytic activities of the as-prepared samples were measured by degrading methyl orange under visible light (λ ≥ 400 nm) irradiation at ambient condition. The light source was a 300 W Xe arc lamp (Beijing Perfectlight Technology Co., Ltd) with a 400 nm cutoff filter. In a typical procedure, 0.2 g photocatalysts were dispersed in 100 ml of a 5 mg/l aqueous solution of MO placed in a beaker. Prior to irradiation, the suspension was magnetically stirred in dark for 30 min to establish adsorption-desorption equilibrium. The experiments were carried out under room air-equilibrated conditions. The light was focused onto the breaker. After visible light irradiation at a given time intervals, 3 ml suspensions were sampled and filtered by membrane filters (0.22 μm pore size). The concentrations of dye aqueous solution were analyzed by UV-vis spectrophotometer (UV-1800, Mapada) at a maximum adsorption wavelength of MO (λ = 464 nm). The photocatalytic performance of TiO₂/PAN, AgBr/PAN and AgI/PAN was also measured under the same conditions.

In order to demonstrate the as-prepared samples could degrade different organic pollutants, the photocatalytic activity of AgX-TiO₂/PAN was measured by monitoring the decomposition of five

RSC Adv.

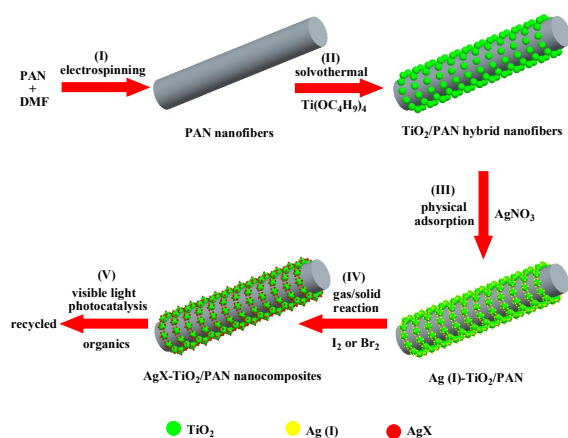
organics (acid red 18, methylene blue, sodium fluorescence, xylenol orange and phenol) aqueous solutions at the same conditions. For detecting the reactive species during photocatalytic degradation, holes (h^+), hydroxyl radicals ($\bullet OH$), superoxide radical ($\bullet O_2^-$) and 1O_2 were investigated by adding 0.2 mM ethylenediamine tetraacetic acid disodium salt (Na_2EDTA), 2 mM isopropanol (IPA), 0.2 mM p-benzoquinone (BQ) and 0.2 mM sodium azide (NaN_3), respectively. The photocatalytic conditions were similar to the above experiments.

To investigate the photochemical stability of the catalysts, the recycling tests of $AgX-TiO_2/PAN$ with the optimum component, which could completely degrade MO, were conducted for five times. At the end of each cycle, the catalysts were collected by filtration, washed with deionized water and dried at 80 °C for 1 h. Then fresh MO solution was mixed with the used catalysts for the next cycle.

Results and discussion

Synthetic procedures

The overall fabrication procedures of $AgX-TiO_2/PAN$ ($X = Br, I$) nanocomposites are illustrated in Scheme 1. It started with the preparation of PAN nanofibers by electrospinning 8 wt% PAN/DMF homogeneous solution, proceeding with dispersing electrospun PAN nanofibers in a $Ti(OC_4H_9)_4$ /ethanol solution and then following to be physical adsorption for 24 h. Then, TiO_2 nanoparticles embedded on PAN nanofibers were fabricated by the alcoholysis of $Ti(OC_4H_9)_4$ during solvothermal process, which promoted the formation of TiO_2 with highly crystallization and uniform size. The as-prepared TiO_2/PAN hybrid nanofibers were added in an $AgNO_3$ aqueous solution and Ag (I) could be absorbed on their surface. Finally, $AgX-TiO_2/PAN$ nanocomposites were fabricated by transforming Ag (I) into AgX through evaporated iodine or bromine.



Scheme 1. Schematic illustration for the preparation of $AgX-TiO_2/PAN$ ($X = Br, I$) nanocomposites.

Catalysts characterization

The crystalline structure of the as-prepared samples was determined by X-ray diffraction (XRD) measurements. XRD patterns of TiO_2/PAN , $AgBr(10\%)-TiO_2/PAN$ and $AgI(10\%)-TiO_2/PAN$ are shown in Fig. 1. All samples exhibited the diffraction peaks of anatase TiO_2 (JCPDS file No. 21-1272), which proved that the solvothermal treatment was beneficial to the formation of anatase TiO_2 .^{29,31,35} The wide peaks appeared in the range of 15° and 20° had been detected, which should be attributed to PAN polymer phase.³⁵ In addition to the diffraction peaks of TiO_2 and PAN, the peaks at $2\theta = 31.28^\circ$ and 44.63° were indexed to $AgBr(200)$ and (220) (JCPDS file No. 06-0438),⁴⁰ while the peak around $2\theta = 22.42^\circ$ should be assigned to $\beta-AgI(100)$ (JCPDS file No. 09-0374).^{6,16,20,21} No other diffraction peaks were displayed in the as-prepared $AgX(10\%)-TiO_2/PAN$. These results revealed that $AgX(X = Br, I)$ nanoparticles could be synthesized by gas/solid reaction.

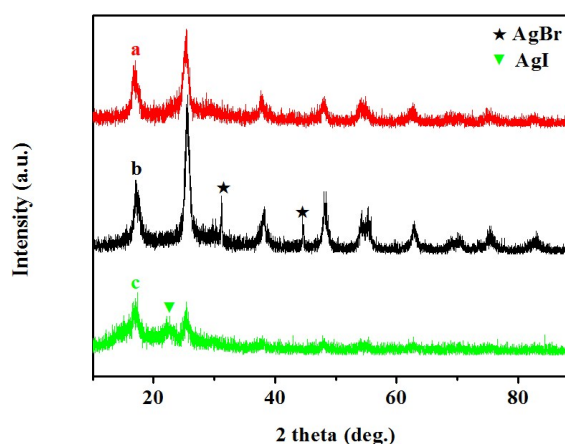


Fig. 1 XRD patterns of (a) TiO_2/PAN , (b) $AgBr(10\%)-TiO_2/PAN$ and (c) $AgI(10\%)-TiO_2/PAN$.

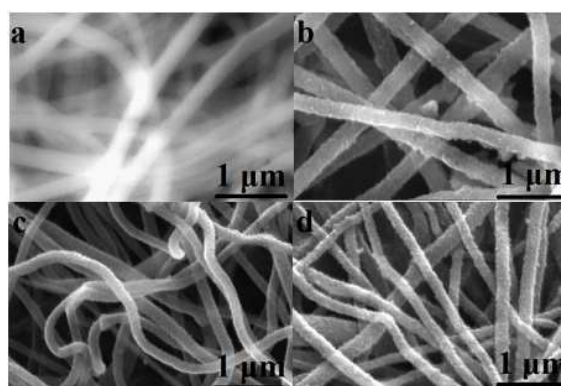


Fig. 2 FE-SEM images of (a) PAN nanofibers, (b) TiO_2/PAN , (c) $AgBr(10\%)-TiO_2/PAN$ and (d) $AgI(10\%)-TiO_2/PAN$.

ARTICLE

RSC Adv.

The microstructures of the obtained samples were examined by field-emission scanning electron microscopy (FE-SEM). Fig. 2a shows the FE-SEM image of PAN nanofibers, which served as supporters in the as-prepared photocatalysts. It could be clearly seen that PAN nanofibers possessed a smooth surface and a uniform diameter. As observed in Fig. 2b, TiO₂/PAN hybrid nanofibers still maintained the morphology and structure of the original PAN nanofibers after solvothermal treatment. Compared with pure PAN nanofibers, uniform TiO₂ nanoparticles were compactly grown on the surface of PAN nanofibers. In consequence, Ag⁺ ions were coupled with TiO₂ nanoparticles rather than PAN nanofibers via physical adsorption process. AgX (X= Br, I) nanoparticles were generated without aggregation via gas/solid reaction (shown in Fig. 2c and d). It could be presumed that AgX nanoparticles had intimate contact with TiO₂.

The morphologies of the obtained samples were determined by TEM images. The low resolution TEM image of TiO₂/PAN was presented in Fig. 3a. Small nanoparticles were uniformly distributed on the surface of PAN nanofibers, while the interplanar spacing of 0.352 nm corresponded to TiO₂ (101) (Fig. 3b),^{40,42} indicating the formation of anatase TiO₂ after solvothermal treatment. As shown in Fig. 3c and d, after modified by AgX (X= Br, I) nanoparticles, no obvious aggregation was found in the AgX-TiO₂/PAN samples. The TEM images (Fig. 3e and f) exhibited the existence of AgX and the HRTEM images (Fig. 3g and h) further confirmed the formation of the heterojunctions between AgX and TiO₂. STEM-HAADP pictures were also used to clarify the distribution of different elements in AgX-TiO₂/PAN nanocomposites (Fig. 4a and b). PAN nanofibers were mainly composed of C and N, which distribution was similar to the structures of composite catalyst. Through the location of Ti and O, it could be presumed TiO₂ nanoparticles were uniformly and densely coated on the surface of PAN nanofibers. There were sporadic signs of Ag and X elements due to their low content.

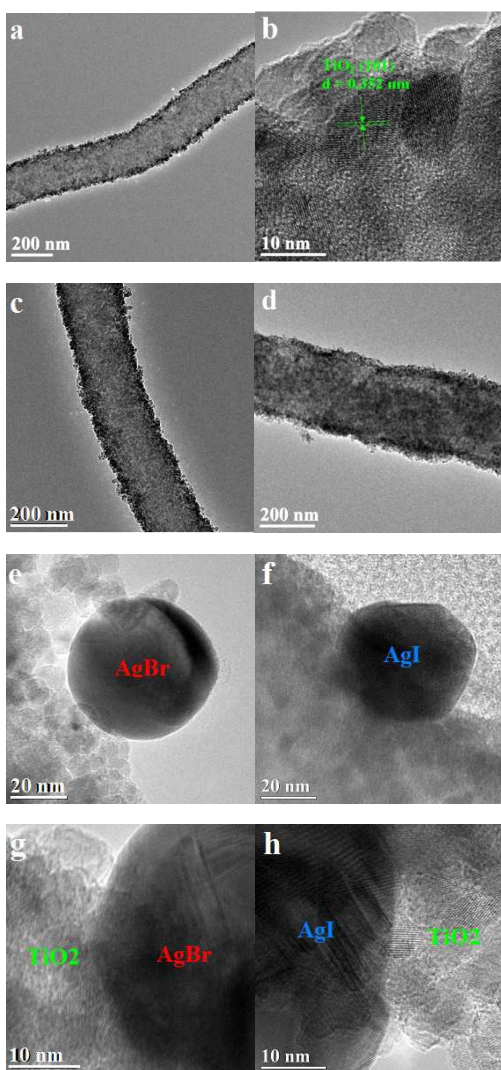


Fig. 3 TEM (a), HRTEM (b) images of TiO₂/PAN (a, b); TEM (c,d,e,f) and HRTEM (g,h) images of AgBr (10%)-TiO₂/PAN (c,e,g) and AgI (10%)-TiO₂/PAN (d, f, h)

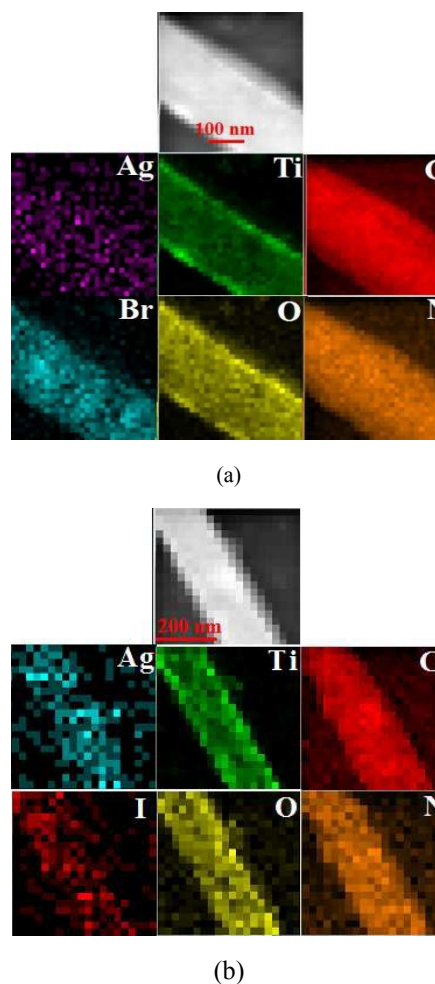


Fig. 4 STEM-HAADF images of the as-prepared AgBr (10%)-TiO₂/PAN(a) and AgI (10%)-TiO₂/PAN (b).

RSC Adv.

Fig. 5 gives the diffuse reflectance UV-vis spectra (DRS) of different photocatalysts. As shown in Fig. 5a and b, two absorption bands presented in the range of 200-300 nm attributing to the contribution of PAN polymer, while a visible-light absorption band could be observed after loading AgX on the surface of PAN nanofibers, especially for AgI, due to the light adsorption of AgX. Fig. 4c exhibits a strong adsorption peak below 390 nm, which should be attributed to the band gap energy of anatase TiO₂ (3.2 eV).^{18,44} Except for the adsorption peak of TiO₂, the as-prepared AgBr-TiO₂/PAN had a little absorption in the visible light region.^{18,42,43,44} Moreover, AgI-TiO₂/PAN exhibited a strong absorption band around 400-436 nm, which should be assigned to the presence of AgI.^{16,19,20} The diffuse reflectance UV-vis spectra future demonstrated the formation of AgX (X= Br, I).

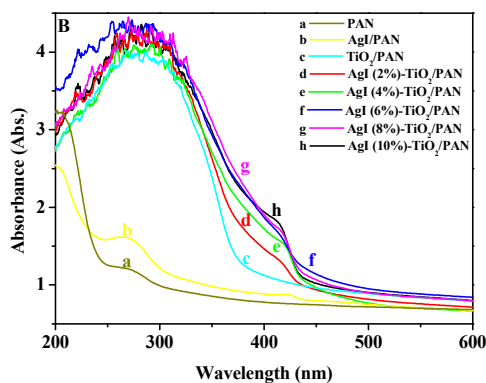
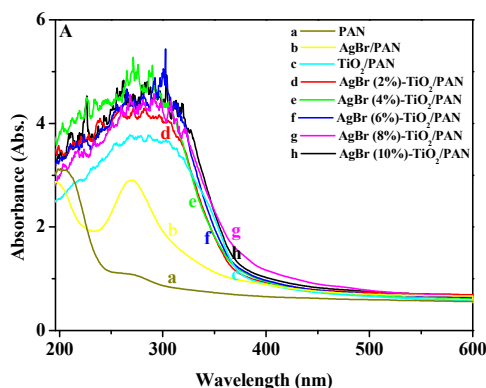


Fig. 5 UV-vis diffuse reflectance spectra of (a) PAN nanofibers, (b) AgX/PAN, (c) TiO₂/PAN and (d)-(h) AgX (γ%)-TiO₂/PAN-n (γ = 2, 4, 6, 8, 10)

The FTIR spectra of pure PAN, TiO₂/PAN, AgBr (10%)-TiO₂/PAN and AgI (10%)-TiO₂/PAN are shown in Fig. 6. The characteristic

absorption peaks at 2244 cm⁻¹ were attributed to the stretching vibration of -C≡N- in PAN.^{39,41} The peak at 1740 cm⁻¹ might originate from the vibration of C=O bonds existed in the hydrolyzed PAN nanofibers or residual DMF.³⁹ In comparison to pure PAN, the FTIR spectra of TiO₂/PAN (Fig. 6b) exhibited a broad absorption band below 1000 cm⁻¹ corresponding to Ti-O-Ti vibration, which proved the formation of TiO₂.⁴² In addition to characteristic absorption peaks of PAN and TiO₂, no different peaks were observed in AgX (10%)-TiO₂/PAN. Furthermore, a shift of the -C≡N- vibration was not detected in AgX (10%)-TiO₂/PAN, which indicated that there was no any bond formation between -C≡N- group in AgX and PAN.⁴¹ So, it could be concluded that AgX nanoparticles did not connect to the PAN nanofibers.

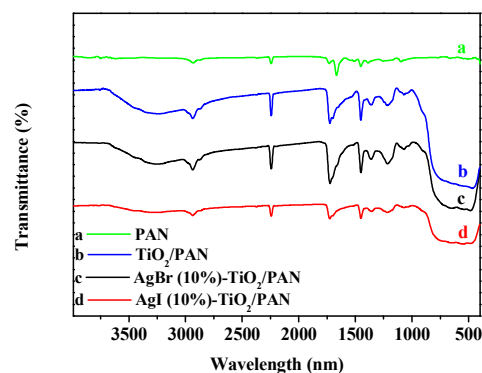


Fig. 6 FTIR spectra of (a) PAN nanofibers, (b) TiO₂/PAN, (c) AgBr (10%)-TiO₂/PAN and (d) AgI (10%)-TiO₂/PAN.

Visible light photocatalytic activity and two-stage photocatalytic mechanism of AgX-TiO₂/PAN

The photocatalytic activities of the as-prepared AgX-TiO₂/PAN were evaluated by visible-light degradation of MO aqueous solution. For comparison, the performances of pure PAN, AgX/PAN and TiO₂/PAN were also investigated. The photodegradation curves of MO over the different samples as a function of visible light irradiation time were plotted in Fig. 7. The degradation rate was represented as the variation of (1-C/C₀) with irradiation time, in which C₀ and C were the concentration of MO at initial time and at certain time interval, respectively. As shown in Fig. 7a, nearly 10% of MO was absorbed by pure PAN nanofibers in dark condition, while the decolorization rate of MO kept unchanged after the light was turned on. It indicated that PAN nanofibers, a supporter in the as-prepared catalysts, only had adsorption ability toward MO, which was beneficial for the degradation of MO. Compared with TiO₂/PAN and AgX/PAN (shown in Fig. 7b and c), AgX-TiO₂/PAN catalysts exhibited the much higher photocatalytic activity. As shown in Fig. 7(d-h), the molar ratios of AgX/TiO₂ had a significant impact on the

ARTICLE

RSC Adv.

photodegradation activity. In the as-prepared AgX-TiO₂/PAN system, when the AgX content increased, the AgX nanoparticles were grown dispersedly on the surface of TiO₂, which was beneficial for the light adsorption. Moreover, the effective contacted interface area between AgX and TiO₂ increased as the AgX ratio rose, promoting the separation of electron-hole pairs.⁴⁷ Thus, the photocatalytic degradation efficiency of MO increased with the AgX loading. As shown in Fig. 7h, most of MO had been removed in the presence of AgX (10%)-TiO₂/PAN after illumination for 4.5 h.

different organics and AgI (10%)-TiO₂/PAN showed much higher photocatalytic activity than AgBr (10%)-TiO₂/PAN for the same organic. Except for phenol solution, the color of organic pollutants gradually diminished as the irradiation time increased, suggesting that the chromophoric groups had been destroyed. It could be presumed that continuing to extend the illumination time, the organics, such as phenol and xylenol orange, could be degraded completely. In summary, the as-prepared AgX-TiO₂/PAN catalysts exhibited the excellent photocatalytic activities for the degradation of methylene blue, sodium fluorescein, phenol, xylenol orange and acid red 18, which could extend their application in the field of degrading different organic pollutants in waste water.

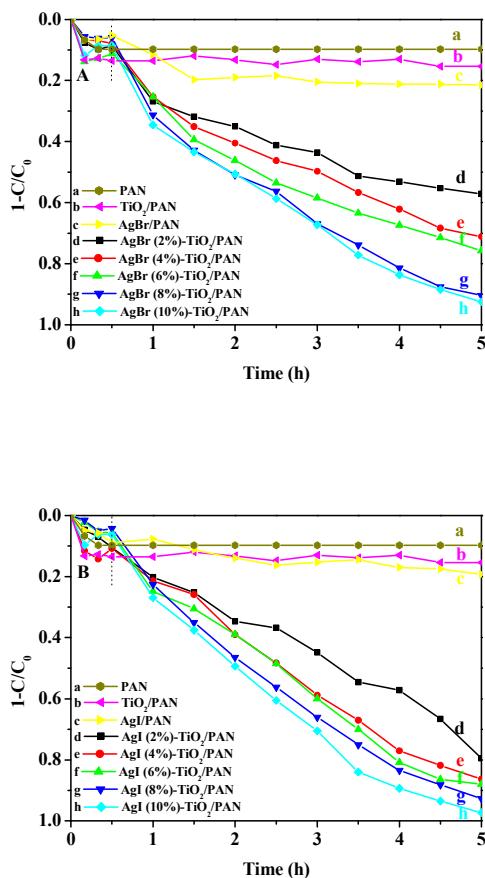


Fig. 7 The degradation curves of MO over (a) PAN, (b) TiO₂/PAN, (c) AgX/PAN and (d)-(h) AgX (γ = 2, 4, 6, 8, 10)

To confirm the universal degradation ability of the as-prepared catalysts, the photocatalytic activities toward different organics were evaluated in the presence of AgBr (10%)-TiO₂/PAN and AgI (10%)-TiO₂/PAN. The degradation curves against irradiation time were plotted in Fig. 8A and B. The initial concentrations of methylene blue, sodium fluorescein, phenol, xylenol orange and acid red 18 were 20mg/l, 20mg/l, 20mg/l, 30mg/l and 5mg/l, respectively. It was clear that the adsorption ability and degradation efficiency of the as-prepared AgX (10%)-TiO₂/PAN varied with

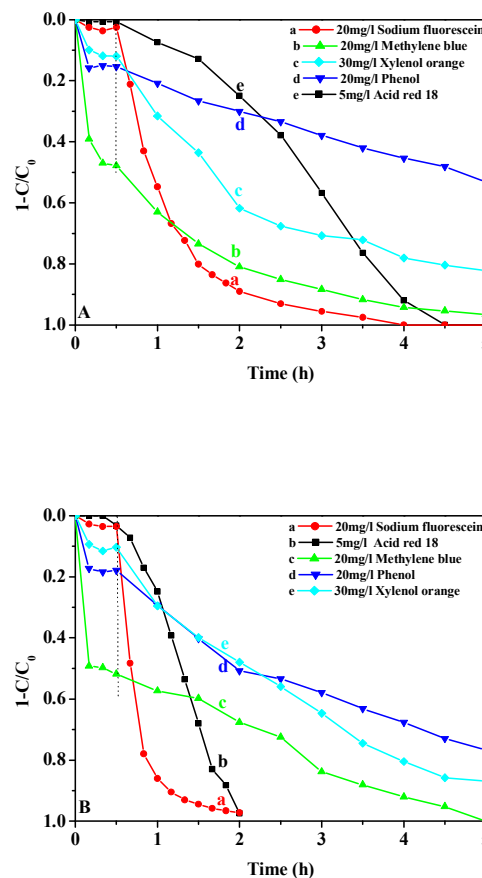


Fig. 8 The adsorption and photodegradation of different organics (100 ml) in aqueous solutions containing 0.2 g AgBr (10%)-TiO₂/PAN (A) or AgI (10%)-TiO₂/PAN (B).

Recycling experiments were carried out to evaluate the stability and durability of AgX (10%)-TiO₂/PAN for MO degradation. Notably, the catalysts could be easily separated from an aqueous solution without any loss due to the application of membranous PAN. In each cycle, the adsorption process was conducted in dark

RSC Adv.

condition for 30 min to establish adsorption-desorption equilibrium and then the irradiation process was lasted for 4.5 h. After 4.5 h of visible light irradiation, the catalysts were filtered, washed with distilled water and dried at 80 °C for 1 h. The recycled tests were performed for five times and described in Fig. 9. A slightly reduction of photocatalytic activity could be observed after the second run, while the degradation efficiency of MO was reduced obviously in the fourth and fifth runs, which was attributed to the photocorrosion of AgX. The decomposition of AgX could be proved by the diffuse reflectance UV-vis spectra (shown in Fig. 10b), in which a strong adsorption band appeared in visible region was attributed to the surface plasma resonance (SPR) of Ag nanoparticles.¹⁵ The catalysts recycled for five times were put in I₂ (or Br₂) atmosphere for regeneration, which could be convinced by the UV-vis DRS of the regenerated AgX-TiO₂/PAN (Fig. 10c). Additional experiments showed that the regenerated catalysts retain high photocatalytic performance. These results demonstrated that the as-prepared AgX-TiO₂/PAN catalysts had a certain photochemical stability and were easily regenerated.

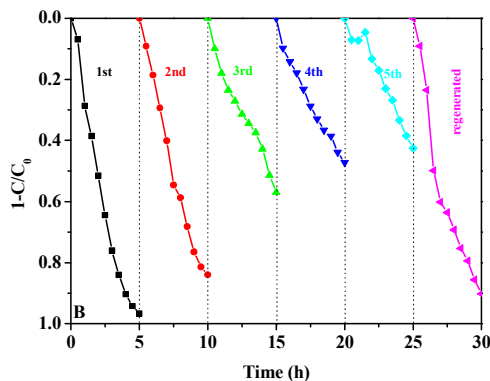
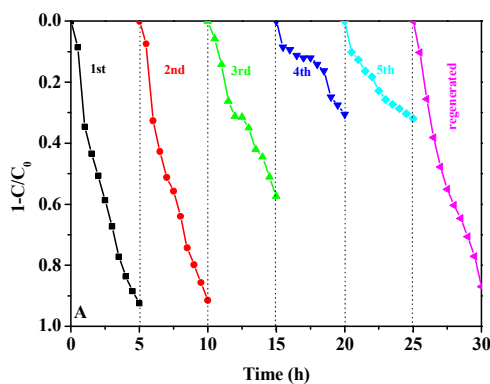


Fig. 9 The cycling degradation efficiency for MO of 0.2 g AgBr (10%)-TiO₂/PAN (A) or AgI (10%)-TiO₂/PAN (B) under visible-light irradiation.

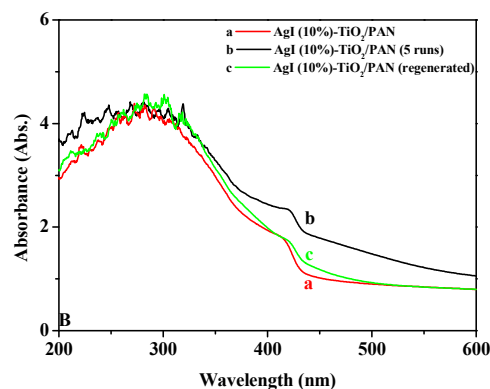
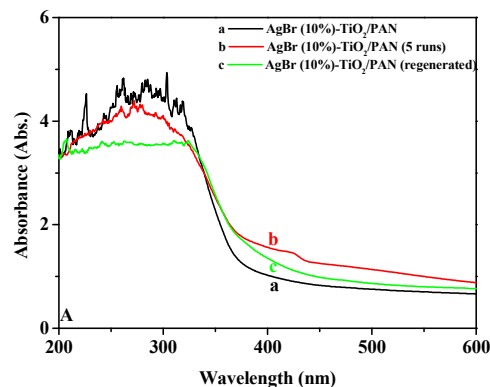


Fig. 10 The UV-vis diffuse reflectance spectra of (a) fresh AgX (10%)-TiO₂/PAN, (b) AgX (10%)-TiO₂/PAN (recycled for five runs) and (c) AgX (10%)-TiO₂/PAN (regenerated).

To illustrate the photocatalytic mechanism of AgX-TiO₂/PAN (X= Br, I), a series of control experiments with different scavengers were carried out to investigate the generation and contribution of reactive species such as h⁺, •OH, •O₂⁻ and ¹O₂, during visible light photocatalysis. In this study, 2 mM IPA was added to quench •OH in the solution,^{16,39} 0.2 mM Na₂EDTA for h⁺,⁴⁷ 0.2 mM BQ for •O₂⁻^{42,43,46,47} and 0.2 mM NaN₃ for ¹O₂.^{42,43} Fig. 11A and B show the photocatalytic degradation curves of MO over AgBr (10%)-TiO₂/PAN and AgI (10%)-TiO₂/PAN in the presence of different scavengers. The addition of NaN₃ and IPA scavengers had a slightly reduction in MO degradation efficiency, which implied that ¹O₂ and •OH were not the main reactive species for MO degradation. The most depressed degradation rate occurred in the presence of Na₂EDTA, indicating that h⁺ was the most significant reactive species. The presence of BQ also dramatically inhibited the removal efficiency of MO, which suggested that •O₂⁻ played an important role in the degradation of

ARTICLE

RSC Adv.

MO.

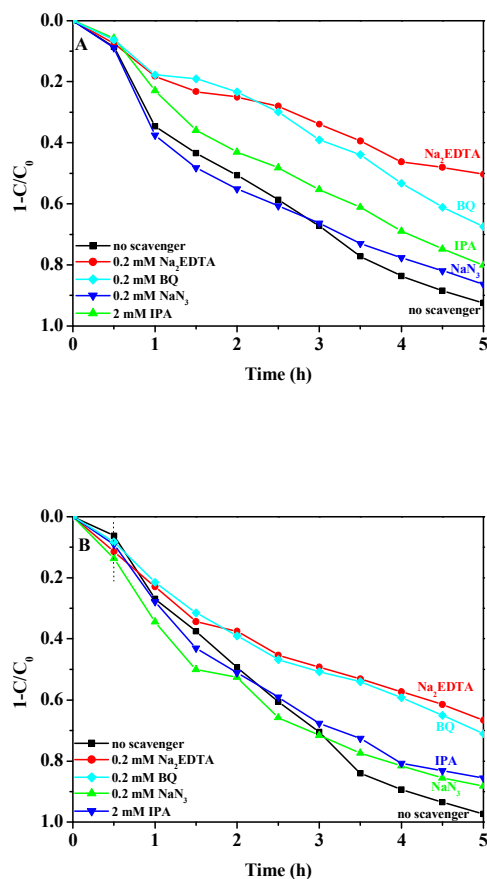
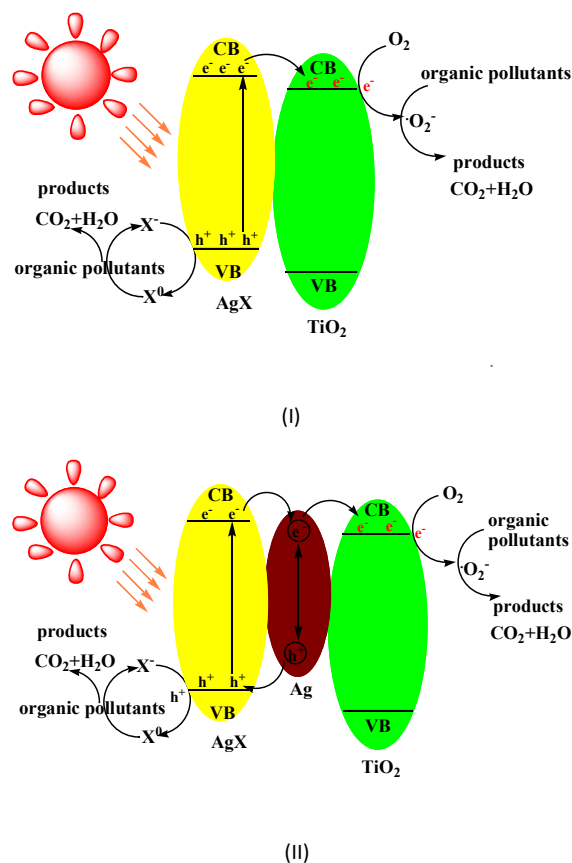


Fig. 11 Photodegradation curves of MO over 0.2 g AgBr (10%)-TiO₂/PAN (A) or AgI (10%)-TiO₂/PAN (B) under visible light irradiation without and with the presence of different scavengers.

On the basis of above experimental results and related researches, the photodegradation mechanism of AgX-TiO₂/PAN (X=Br, I) under visible light irradiation was proposed and illustrated in Scheme 2. The photocatalytic process could be divided into two stages for the decomposition of AgX. At the first stage, under visible light irradiation, AgX nanoparticles could be excited to produce photoinduced electrons (e⁻) and holes (h⁺), due to their narrow band gap (AgBr, 2.6 eV; AgI, 2.8 eV).^{43,48} The generated e⁻ in AgX could migrate to the conduction band (CB) of TiO₂ for the less negative CB of TiO₂ as compared to that of AgX.^{48,49} Then the electrons would be trapped by surface absorbed O₂ to form •O₂⁻ and reactive oxygen species such as •OH and ¹O₂ could be further generated. The left holes (h⁺) might transfer to the interface between AgX and TiO₂ and oxidize X⁻ to X⁰. X⁰ could oxidize organic pollutants while being reduced to X⁻. X⁻ could oxidize organic pollutants while being reduced to X⁻. Meanwhile, •O₂⁻, •OH and ¹O₂ also had a strong oxidizing ability to degrade organic pollutants. Therefore, the efficient separation of electron-hole pairs was achieved, which facilitated the photocatalytic degradation of

organics. The relevant reactions could be shown in Table 1.

As the illumination time extended, AgX could be decomposed into Ag⁰. Therefore, fresh AgX-TiO₂/PAN was turned into Ag-AgX-TiO₂/PAN. In the newly constructed system, the electron-hole pairs could also be formed in Ag⁰ owing to their surface plasmon resonance (SPR) under visible light irradiation.^{42,43,45,46} Considering the SPR-induced local electromagnetic field and the polarization effect of negatively charged AgX surface, the photoinduced electrons and holes from Ag⁰ would migrate to the completely different directions. The photoinduced electrons in Ag⁰ might migrate to the conduction band of TiO₂, while the holes would transfer from Ag⁰ to valance band of AgX particles, leading to the efficient separation of electron-hole pairs in the Ag⁰.^{42,43,50} Besides, the electrons generated from AgX could be injected into Ag⁰ and immediately migrate to the CB of TiO₂.^{42,43} The electrons transferred from AgX could significantly inhibit the reaction where Ag⁺ ions of AgX might capture the electrons generated in the CB of AgX, resulting in the decomposition of AgX.⁴³ The generation process of reactive species in this system was similar to that of fresh AgX-TiO₂/PAN. The major reaction steps were summarized in Table 2. As for the regenerated catalysts, charge transfer in photocatalytic process would go through the same procedure occurred in fresh AgX-TiO₂/PAN.



Scheme 2. Schematic illustration of two-stage photocatalytic mechanism within AgX-TiO₂/PAN under visible light irradiation.

RSC Adv.

Table 1. Relevant reactions happened in the first stage of photocatalytic process

Reactions	No.
$\text{AgX} + \text{h}\nu \rightarrow \text{AgX} (\text{e}^- + \text{h}^+)$	(1)
$\text{AgX} (\text{e}^- + \text{h}^+) + \text{TiO}_2 \rightarrow \text{AgX} (\text{h}^+) + \text{TiO}_2 (\text{e}^-)$	(2)
$\text{TiO}_2 (\text{e}^-) + \text{O}_2 \rightarrow \bullet\text{O}_2^- + \text{TiO}_2$	(3)
$\bullet\text{O}_2^- + \text{H}^+ \rightarrow \text{HO}_2\bullet$	(4)
$\text{HO}_2\bullet + \text{TiO}_2 (\text{e}^-) + \text{H}^+ \rightarrow \text{H}_2\text{O}_2 + \text{TiO}_2$	(5)
$\text{H}_2\text{O}_2 + \text{TiO}_2 (\text{e}^-) \rightarrow \bullet\text{OH} + \text{OH}^- + \text{TiO}_2$	(6)
$\bullet\text{O}_2^- + \bullet\text{OH} \rightarrow {}^1\text{O}_2 + \text{OH}^-$	(7)
$\text{AgX} (\text{h}^+) + \text{X}^- \rightarrow \text{AgX} + \text{X}^0$	(8)
$\text{X}^0 + \text{organics} \rightarrow \text{products} + \text{X}^-$	(9)
$\bullet\text{O}_2^-, \bullet\text{OH}, {}^1\text{O}_2 + \text{organics} \rightarrow \text{products}$	(10)

Table 2. Major reaction steps happened in the second stage of photocatalytic process.

Reactions	No.
$\text{AgX} + \text{h}\nu \rightarrow \text{AgX} (\text{e}^- + \text{h}^+)$	(1)
$\text{Ag}^0 + \text{h}\nu \rightarrow \text{Ag}^*$	(2)
$\text{Ag}^* + \text{h}\nu \rightarrow \text{TiO}_2 (\text{e}^-) + \bullet\text{Ag}^+$	(3)
$\bullet\text{Ag}^+ + \text{AgX} \rightarrow \text{Ag}^0 + \text{AgX} (\text{h}^+)$	(4)
$\text{AgX} (\text{h}^+) + \text{X}^- \rightarrow \text{AgX} + \text{X}^0$	(5)
$\text{X}^0 + \text{organics} \rightarrow \text{products} + \text{X}^-$	(6)
$\text{TiO}_2 (\text{e}^-) + \text{O}_2 \rightarrow \bullet\text{O}_2^- + \text{TiO}_2$	(7)
$\bullet\text{O}_2^- + \text{H}^+ \rightarrow \text{HO}_2\bullet$	(8)
$\text{HO}_2\bullet + \text{TiO}_2 (\text{e}^-) + \text{H}^+ \rightarrow \text{H}_2\text{O}_2 + \text{TiO}_2$	(9)
$\text{H}_2\text{O}_2 + \text{TiO}_2 (\text{e}^-) \rightarrow \bullet\text{OH} + \text{OH}^- + \text{TiO}_2$	(10)
$\bullet\text{O}_2^- + \bullet\text{OH} \rightarrow {}^1\text{O}_2 + \text{OH}^-$	(11)
$\bullet\text{O}_2^-, \bullet\text{OH}, {}^1\text{O}_2 + \text{organics} \rightarrow \text{products}$	(12)

Conclusions

Novel visible light photocatalysts $\text{AgX-TiO}_2/\text{PAN}$ ($\text{X} = \text{Br}, \text{I}$) with different molar ratios between AgX and TiO_2 were synthesized via a facile electrospinning technique, solvothermal synthesis, physical adsorption and gas/solid reaction. In the as-prepared catalysts, TiO_2

nanoparticles were densely and uniformly distributed on the surface of PAN nanofibers and AgX nanoparticles were closely combined with TiO_2 rather than PAN nanofibers. The fabricated catalysts exhibited a highly visible light photocatalytic performance in degrading different organics. But most of all, they could be easily separated and regenerated. Based on the experimental results, a possible photocatalytic process was also proposed. It could be concluded that the high photocatalytic activity of $\text{AgX-TiO}_2/\text{PAN}$ was attributed to the well contact between AgX and TiO_2 and the efficient separation of photogenerated electron-hole pairs. The excellent photocatalytic performance and reusable property of $\text{AgX-TiO}_2/\text{PAN}$ enabled it to be a promising material in the field of environmental remediation.

Acknowledgements

The authors gratefully acknowledge the support from the National Natural Science Foundation of China (no. 21266016) and Specialized Research Fund for the Doctoral Program of Higher Education (no. 20121514120004).

References

- S. Q. Liu, Z.-R. Tang, Y. G. Sun, J. C. Colmenares and Y.-J. Xu, *Chem. Soc. Rev.*, 2015, **44**, 5053.
- Z. F. Bian, T. Tachikawa, P. Zhang, M. Fujitsuka and T. Majima, *J. Am. Chem. Soc.*, 2014, **136**, 458.
- W.-S. Wang, H. Du, R.-X. Wang, T. Wen and A.-W. Xu, *Nanoscale*, 2013, **5**, 3315.
- N. Zhang, M.-Q. Yang, S. Q. Liu, Y. G. Sun and Y.-J. Xu, *Chem. Rev.* 2015, **115**, 10307.
- H. F. Cheng, B. B. Huang, Y. Dai, X. Y. Qin and X. Y. Zhang, *Langmuir*, 2010, **26**(9), 6618.
- C. H. An, W. Jiang, J. Z. Wang, S. T. Wang, Z. H. Ma and Y. P. Li, *Dalton Trans.*, 2013, **42**, 8796.
- X. Liu, Y. X. Li, S. Q. Peng, G. X. Lu and S. B. Li, *Photochem. Photobiol. Sci.*, 2013, **12**, 1903.
- D. Dvoranová, V. Brezová, M. Mazúr and M. A. Malati, *Appl. Catal., B*, 2002, **37**, 91.
- C. Han, M.-Q. Yang, N. Zhang and Y.-J. Xu, *J. Mater. Chem. A*, 2014, **2**, 19156.
- N. Serpone, *J. Phys. Chem. B*, 2006, **110**, 24287.
- H. Wang, T. T. You, W. W. Shi, J. H. Li and L. Guo, *J. Phys. Chem. C*, 2012, **116**, 6490.
- W.-T. Sun, Y. Yu, H.-Y. Pan, X.-F. Gao, Q. Chen and L.-M. Peng, *J. Am. Chem. Soc.*, 2008, **130**, 1124.
- H. Wang, J. T. Yang, X. L. Li, H. Z. Zhang, J. H. Li and L. Guo, *Small*, 2012, **8** (18), 2802.
- H. Xu, J. Yan, Y. G. Xu, Y. H. Song, H. M. Li, J. X. Xia, C. J. Huang and H. L. Wan, *Appl. Catal., B*, 2013, **129**, 182.
- P. Wang, B. B. Huang, X. Y. Zhang, X. Y. Qin, H. Jin, Y. Dai, Z. Y. Wang, J. Y. Wei, J. Zhan, S. Y. Wang, J. P. Wang and M.-H. Whangbo, *Chem. Eur. J.*, 2009, **15**, 1821.
- C. Hu, X. X. Hu, L. S. Wang, J. H. Qu and A. M. Wang, *Environ. Sci. Technol.*, 2006, **40**, 7903.
- P. W. Huo, Y. S. Yan, S. T. Li, H. M. Li and W. H. Huang, *Desalination*, 2010, **256**, 196.
- Q. Y. Li, Y. Y. Xing, R. Li, L. L. Zong, X. D. Wang and J. J. Yang, *RSC Adv.*, 2012, **2**, 9781.
- D. Y. Wu and M. C. Long, *ACS Appl. Mater. Interfaces*, 2011, **3**, 4770.

ARTICLE

RSC Adv.

- 20 Y. Z. Li, H. Zhang, Z. M. Guo, J. J. Han, X. J. Zhao, Q. N. Zhao and S.-J. Kim, *Langmuir*, 2008, **24**, 8351.
- 21 W. Sun, Y. Z. Li, W. Q. Shi, X. J. Zhao and P. F. Fang, *J. Mater. Chem.*, 2011, **21**, 9263.
- 22 C. Hu, J. Guo, J. H. Qu and X. X. Hu, *Langmuir*, 2007, **23**, 4982.
- 23 M. Pirhashemi and A. Habibi-Yangjeh, *J. Alloys Compd.*, 2014, **601**, 1.
- 24 J. Li, W. W. Tu, H. B. Li, J. C. Bao and Z. H. Dai, *Chem. Commun.*, 2014, **50**, 2108.
- 25 K. Vignesh, A. Suganthi, M. Rajarajan and S. A. Sara, *Powder Technol.*, 2012, **224**, 331.
- 26 L. Q. Ye, J. Y. Liu, C. Q. Gong, L. H. Tian, T. Y. Peng and L. Zan, *ACS Catal.*, 2012, **2**, 1677.
- 27 L. Kong, Z. Jiang, H. H. Lai, R. J. Nicholls, T. C. Xiao, M. O. Jones and P. P. Edwards, *J. Catal.*, 2012, **293**, 116.
- 28 C. Prahsarn, W. Klinsukhon and N. Roungpaisan, *Mater. Lett.*, 2011, **65**, 2498.
- 29 C. Y. Su, Y. F. Tong, M. Y. Zhang, Y. Zhang and C. L. Shao, *RSC Adv.*, 2013, **3**, 7503.
- 30 Y. Y. Liang, H. L. Wang, H. S. Casalongue, Z. Chen and H. J. Dai, *Nano Res.*, 2010, **3**, 701.
- 31 S. Izadyar and S. Fatemi, *Ind. Eng. Chem. Res.*, 2013, **52**, 10961.
- 32 H.-W. Liang, W.-J. Zhang, Y.-N. Ma, X. Cao, Q.-F. Guan, W.-P. Xu and S.-H. Yu, *ACS Nano*, 2011, **5**(10), 8148.
- 33 K. Woan, G. Pyrgiotakis and W. Sigmund, *Adv. Mater.*, 2009, **21**, 2233.
- 34 Y. H. Zhang, Z.-R. Tang, X. Z. Fu and Y.-J. Xu, *ACS Nano*, 2010, **4**(12), 7303.
- 35 C. Y. Su, X. Ran, J. L. Hu and C. L. Shao, *Environ. Sci. Technol.*, 2013, **47**, 11562.
- 36 H. C. Yu, Q. S. Dong, Z. B. Jiao, T. Wang, J. T. Ma, G. X. Lu and Y. P. Bi, *J. Mater. Chem. A*, 2014, **2**, 1668.
- 37 S. K. Nataraj, K. S. Yang and T. M. Aminabhavi, *Prog. Polym. Sci.*, 2012, **37**, 487.
- 38 J. Bai, Y. X. Li, S. T. Yang, J. S. Du, S. G. Wang, C. Q. Zhang, Q. B. Yang and X. S. Chen, *Nanotechnology*, 2007, **18**, 305601.
- 39 Y. C. Chou, C. L. Shao, X. H. Li, C. Y. Su, H. C. Xu, M. Y. Zhang, P. Zhang, X. Zhang, Y. C. Liu, *Appl. Surf. Sci.*, 2013, **285P**, 509-516.
- 40 X. P. Wang and T.-T. Lim, *Water Res.*, 2013, **47**, 4148.
- 41 G. Panthi, S.-J. Park, T.-W. Kim, H.-J. Chung, S.-T. Hong, M. Park and H.-Y. Kim, *J. Mater. Sci.*, 2015, **50**, 4477.
- 42 P. H. Wang, Y. X. Tang, Z. L. Dong, Z. Chen and T.-T. Lim, *J. Mater. Chem. A*, 2013, **1**, 4718.
- 43 X. P. Wang, Y. X. Tang, Z. Chen and T.-T. Lim, *J. Mater. Chem.*, 2012, **22**, 23149.
- 44 C. Hu, Y. Q. Lan, J. H. Qu, X. X. Hu and A. M. Wang, *J. Phys. Chem. B*, 2006, **110**, 4066.
- 45 J. G. Yu, G. P. Dai and B. B. Huang, *J. Phys. Chem. C*, 2009, **113**, 16394.
- 46 B. Z. Tian, R. F. Dong, J. M. Zhang, S. Y. Bao, F. Yang and J. L. Zhang, *Appl. Catal., B*, 2014, **158-159**, 76.
- 47 L. Yin, Z. Wang, L. Lu, X. K. Wan and H. X. Shi, *New J. Chem.*, 2015, **39**, 4891.
- 48 J. H. Yi, L. L. Huang, H. J. Wang, H. Yu, F. Peng, *J. Hazard. Mater.* 2015, **284**, 207.
- 49 M. A. Asi, C. He, M. H. Su, D. H. Xia, L. Lin, H. Q. Deng, Y. Xiong, R. L. Qiu, X.-Z. Li, *Catal. Today*, 2011, **175**, 256.
- 50 D. D. Yu, J. Bai, H. O. Liang, J. Z. Wang and C. P. Li, *Appl. Surf. Sci.*, 2015, **349**, 241.